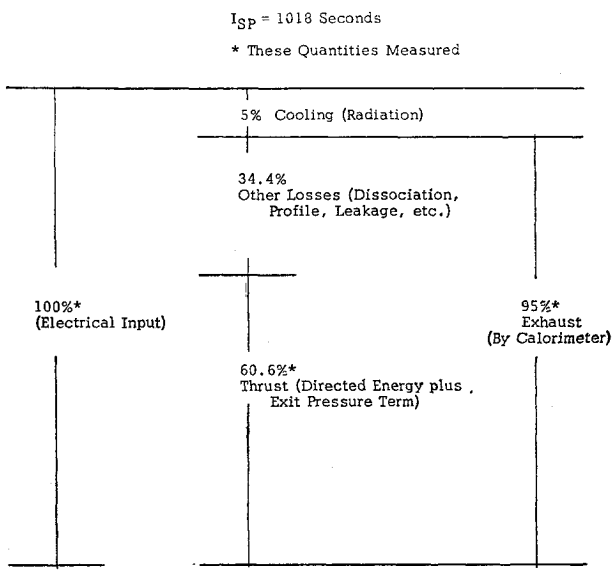

Fig. 3 Typical H-100-F thrustor energy balance

of the throat. The experimental results indicate that the arc usually did strike in the desired place, and that the given geometry of subsonic arc chamber, immediately followed by a throat and expanding nozzle, did give relatively uniform flow and some recombination.

A typical experimental energy balance for this thrustor is shown in Fig. 3. The value of 60.6% of the electrical input appearing as directed energy is approximately equal to the ideal efficiency for frozen flow. When heat transfer, profile loss, and frictional loss are considered, it appears that some recombination was occurring. It is felt that this is due at least partly to the convergent-divergent geometry used where there is a low-velocity, high-density region that serves to promote recombination and also acts as a "trap" for nonequilibrium electrons. The low cooling loss of approximately 5% indicates that fairly effective regenerative cooling was being achieved (by conduction through the electrode and nozzle), since the electrical anode heating plus conduction should be considerably greater than 5%. The other losses of 34.4% due to dissociation, profile, leakage, etc., appear to be consistent with the assumption of reasonable profiles and a freezing-point pressure of about 1 atm.

Life has not been a prime goal of this effort; however, the results obtained with a tungsten insert in the H-100-F thrustor appear to be promising. This insert has been operated for approximately 4 hr at about 1000 sec with less than 0.1% change in diameter, thus indicating a life of about 30 hr. There is strong evidence that with more direct regenerative cooling this can be increased to 100 to 500 hr at 1000 sec.

Conclusions

1) It is possible to obtain over 50% efficiency at 1000-sec specific impulse using hydrogen in the hot-wall thrustor described. This geometry appears to give a relatively uniform exhaust, good operating stability, and some recovery of dissociation energy. However, considerably more experimental effort will be required before the results will be understood well.

2) Complete regenerative cooling with negligible external energy loss at 1000 sec appears possible with hydrogen as propellant by combining the features of the H-100-C and H-100-F thrustors. The potential efficiency is about 70% at 1000 sec.

References

[1] Masser, P. S., "Recent experimental plasmajet thrustor results." ARS-IAS Preprint 61-100-1794 (June 1961).

[2] Masser, P. S., "Development of a thermal arc engine," Plasmadyne, Final Rept. on Contract AF 33(616)-7112 (April 1961).

[3] Masser, P. S., Page, R. J., and Stoner, W. A., "A preliminary engineering evaluation of advanced space propulsion systems," *Generalized Propulsion System Analysis and Mission Requirements*, Vol. I, Air Force Wright Air Dev. Center TR-59-189(I), Contract AF33(616)-5709 (March 1959).

[4] Masser, P. S., Page, R. J., and Stoner, W. A., "Electrical thrust devices for propulsion," Plasmadyne, Contract DA-04-495-ORD-1032 (September 1959).

[5] Stoner, W. A., "Investigation of a low-thrust plasma propulsion device," Plasmadyne, Final Tech. Summary Rept. on Contract DA-04 495-21X4992, 506-ORD-1806 (February 1961).

[6] Page, R. J., Buhler, R. D., Stoner, W. A., and Masser, P. S., "Arc plasma thrustor studies," ARS Preprint 1508-60 (December 1960).

Deflections of an Inflated Circular-Cylindrical Cantilever Beam

R. L. Comer*
General Electric Company, Daytona Beach, Fla.

AND

Samuel Levy†
General Electric Company, Schenectady, N. Y.

Nomenclature

l = beam length, in.
R = cylinder radius, in.
t = wall thickness, in.
A = cross-sectional area, in.^{2}
p = internal pressure, lb/in.^{2}
P = lateral load at tip, lb
q = distributed lateral load
E = Young's modulus, lb/in.^{2}
G = shear modulus, lb/in.^{2}
d_b = tip deflection due to bending, in.
d_s = tip deflection due to shear, in.
σ = stress, lb/in.^{2}
σ_M = maximum stress in axial direction, lb/in.^{2}
σ_0 = minimum stress in axial direction, lb/in.^{2}
y = lateral deflection of beam, in.
x = distance from loaded end, in.
θ,θ_0 = angular positions

I. Introduction

THE use of inflatable structures for applications in space suggests itself because of their low weight and their suitability for light loads. A discussion of such space structures is given by Leonard, Brooks, and McComb.[1] Among the structures they consider is the inflated circular-cylindrical tube acting as a cantilever. They derive an equation for the collapse load of such a beam on the assumption that at failure the root folds like a plastic hinge. On this basis they show that the maximum tip load carried is $P = \pi pR^3/l$, where p is the internal pressure. They obtain test data that are in agreement with this equation. An inflated circular-cylindrical tube carrying a constant moment is considered by Stein and Hedgepeth.[2] They obtain a relationship between beam curvature and moment. Other inflatable structures are discussed by Topping[3] and Harris and Stimler.[4] Buckling

Presented at the ARS 17th Annual Meeting and Space Flight Exposition, Los Angeles, Calif., November 13–18, 1962; revision received April 30, 1963.

* Engineer, Command Systems Division, Apollo Support Department.

† Senior Mechanical Engineer, Advanced Technology Laboratories. Member AIAA.

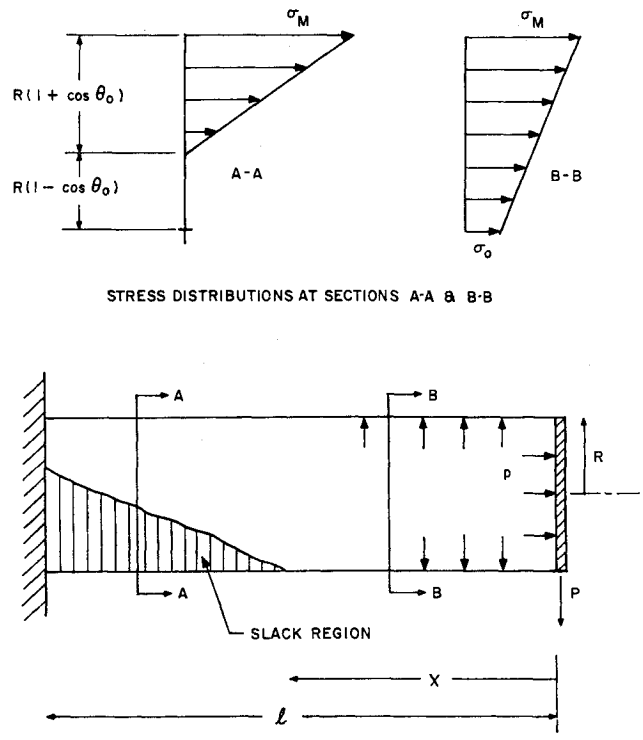

Fig. 1 Inflated circular-cylindrical cantilever beam

of inflated circular-cylindrical shells of appreciable wall thickness is analyzed in Refs. 5–10. These analyses show that for very thin-walled cylinders buckling begins as soon as the stress becomes compressive.

Incipient buckling begins[1] at a load for which the bending stress just cancels the axial stress due to pressure. As the load increases beyond this value, the tube wall becomes slack in an axial direction over an increasing area. When the slackness extends completely around the root cross section, collapse takes place.

The present paper considers the beam deflections and stresses for loads between incipient buckling and final collapse. It is based on the assumption that the internal pressure maintains the circular shape. It assumes also that plane sections remain plane.

II. Analysis

The stress distributions in the slack and in the taut regions of an inflated circular-cylindrical cantilever beam are shown in Fig. 1. In the slack region, the stress is zero in an axial direction. The angle θ_0 is zero for $x < (\pi pR^3/2P)$. For values of x greater than this, θ_0 is greater than zero. Above the angle θ_0 the stress increases linearly to a maximum value σ_M so that the stress σ at other angles is given by

$$\left.\begin{aligned} \sigma &= \left(\frac{\cos\theta_0 - \cos\theta}{1+\cos\theta_0}\right)\sigma_M \qquad \pi > \theta > \theta_0 \\ \sigma &= 0 \qquad\qquad \theta_0 > \theta > 0 \qquad \text{slack region} \end{aligned}\right\} \frac{\pi pR^3}{2P} < x < l \tag{1}$$

A. Beam with tip load

For balance of moments about a transverse axis through the center of the cylinder at a distance x from the tip, one has

$$Px = -2\int_0^\pi t\sigma R^2 \cos\theta d\theta \tag{2}$$

For those values of x for which θ_0 is greater than zero, i.e., $(\pi pR^3/2P) < x < l$, Eqs. (1) and (2) give

$$\sigma_M = \frac{2Px(1+\cos\theta_0)}{tr^2\,(2\pi - 2\theta_0 + \sin 2\theta_0)} \qquad \frac{\pi pR^3}{2P} < x < l \tag{3}$$

For balance of axial forces exerted by the internal pressure on the endplate, one has

$$p\pi R^2 = 2\int_0^\pi t\sigma R d\theta \tag{4}$$

With (1), this gives

$$\sigma_M = \frac{\pi pR(1+\cos\theta_0)}{2t\,[\sin\theta_0 + (\pi - \theta_0)\cos\theta_0]} \qquad \frac{\pi pR^3}{2P} < x < l \tag{5}$$

Equating the values of σ_M in Eqs. (3) and (5) gives

$$\frac{Px}{pR^3} = \frac{\pi(2\pi - 2\theta_0 + \sin 2\theta_0)}{4[\sin\theta_0 + (\pi - \theta_0)\cos\theta_0]} \qquad \frac{\pi pR^3}{2P} < x < l \tag{6}$$

It should be noted in Eq. (6) that $\theta_0 = 0$ gives $(Px/pR^3) = \pi/2$. As $\theta_0 \to \pi$, the value of $(Px/pR^3) \to \pi$. This determines the value of the collapse load when $x = l$. These values are in agreement with results in Ref. 1.

In the region $0 < x < (\pi pR^3/2P)$ of an inflated circular-cylindrical cantilever beam, the stress increases from σ_0 at an angle $\theta = 0$ to σ_M at $\theta = \pi$. The stress is given by

$$\sigma = \sigma_0\,(1+\cos\theta)/2 + \sigma_M(1-\cos\theta)/2 \qquad 0 < x < (\pi pR^3/2P) \tag{7}$$

Substituting the value of σ in Eq. (7) into Eq. (2) and integrating gives

$$\sigma_M - \sigma_0 = (2Px)/(\pi tR^2) \qquad 0 < x < (\pi pR^3/2P) \tag{8}$$

Substituting the value of σ in Eq. (7) into Eq. (4) and integrating gives

$$\sigma_M + \sigma_0 = pR/t \qquad 0 < x < (\pi pR^3/2P) \tag{9}$$

Combining (8) and (9) gives

$$\sigma_M = (pR)/(2t) + (Px)/(tR^2\pi) \qquad 0 < x < (\pi pR^3/2P) \tag{10}$$

The curvature in the region $(\pi pR^3/2P) < x < l$ is given by

$$\text{curvature} = \frac{(\sigma_M/E)}{R(1+\cos\theta_0)} \qquad \frac{\pi pR^3}{2P} < x < l \tag{11}$$

Setting the curvature equal to d^2y/dx^2 and substituting for σ_M the value given by Eq. (3) gives

$$\frac{d^2y}{dx^2} = \left(\frac{Px}{EtR^3}\right)\left(\frac{2}{2\pi - 2\theta_0 + \sin 2\theta_0}\right) \qquad \frac{\pi pR^3}{2P} < x < l \tag{12}$$

The curvature in the region $0 < x < (\pi pR^3/2P)$ is given by

$$\text{curvature} = \frac{(\sigma_M - \sigma_0)}{2RE} \qquad 0 < x < \frac{\pi pR^3}{2P} \tag{13}$$

Setting this equal to d^2y/dx^2 and substituting the value of $(\sigma_M - \sigma_0)$ in Eq. (8) gives

$$d^2y/dx^2 = Px/EtR^3\pi \qquad 0 < x < (\pi pR^3/2P) \tag{14}$$

The integration of Eqs. (12) and (14) to get the deflection is obtained readily if use is made of the dimensionless variables

$$\left.\begin{aligned} \eta &= (P^2Et/p^3R^6)\,y \\ \xi &= (P/pR^3)\,x \end{aligned}\right\} \tag{15}$$

Equations (6, 12, and 14) then become

$$\frac{2\pi - 2\theta_0 + \sin 2\theta_0}{\sin\theta_0 + (\pi - \theta_0)\cos\theta_0} = \frac{4\xi}{\pi} \qquad \pi > \xi > \frac{\pi}{2} \tag{16}$$

$$\frac{d^2\eta}{d\xi^2} = \xi\left(\frac{2}{2\pi - 2\theta_0 + \sin\theta_0}\right) \qquad \pi > \xi > \frac{\pi}{2} \tag{17}$$

$$\frac{d^2\eta}{d\xi^2} = \frac{\xi}{\pi} \qquad \frac{\pi}{2} > \xi > 0 \tag{18}$$

Equations (17) and (18) were integrated numerically using Eq. (16) to obtain values of θ_0 to be used in (17). The boundary condition at the root, $x = l$, ($\xi = Pl/pR^3$), was taken as $\eta = 0$ and $d\eta/d\xi = 0$. In Fig. 2, curve A gives the dimensionless tip deflection thus computed as $(Et\ d_b/pl^2) = \eta_0(pR^3/Pl)^2$, where η_0 is the value of η when $\xi = 0$.

The maximum stress in the beam is obtained readily in dimensionless form from Eqs. (3) and (10) as

$$\frac{tR^2\sigma_M}{Pl} = \left(\frac{pR^3\xi}{Pl}\right)\left[\frac{2(1+\cos\theta_0)}{2\pi - 2\theta + \sin 2\theta_0}\right] \qquad \pi > \xi > \frac{\pi}{2} \tag{19}$$

$$\frac{tR^2\sigma_M}{Pl} = \left(\frac{pR^3}{Pl\pi}\right)\left(\xi + \frac{\pi}{2}\right) \qquad \frac{\pi}{2} > \xi > 0 \tag{20}$$

In Fig. 2, curve B gives the dimensionless stress $(t\sigma_M/pR) = (tR^2\sigma_M/Pl)(Pl/pR^3)$ at the root of the beam, $x = l$, ($\xi = Pl/pR^3$), determined from Eqs. (19) and (20), with (16) used to compute θ_0.

In general, shearing deflections in an inflated cylindrical cantilever beam will be small so long as the length is substantially more than the radius:

$$d_s \ll d_b \text{ when } R \ll l \tag{21}$$

In those instances where the length is comparable to the radius, the shearing deflection can be computed from

$$(dy/dx)_{\text{shear}} = -1.5P/AG \tag{22}$$

where A is the entire cross-sectional area in the region $0 < x < (\pi pR^3/2P)$ and A is only the cross-sectional area above $\theta = \theta_0$ in the region $(\pi pR^3/2P) < x < l$. The form factor 1.5 is an approximation for the ratio of shearing stress at the neutral axis to average shearing stress. The use of a more accurate value did not seem to be warranted. Then one has

$$A = 2tR(\pi - \theta_0) \qquad \pi > \xi > \pi/2 \tag{23}$$

$$A = 2\pi tR \qquad \pi/2 > \xi > 0 \tag{24}$$

If a dimensionless notation is used

$$\zeta = (tE/pR^2)y_{(\text{shear})} \tag{25}$$

and $G = E/2(1+\nu) = E/2.6$, one gets for (22)

$$d\zeta/d\xi = -1.95/(\pi - \theta_0) \qquad \pi > \xi > \pi/2 \tag{26}$$

$$d\zeta/d\xi = -1.95/\pi \qquad \pi/2 > \xi > 0 \tag{27}$$

Equations (26) and (27) were integrated numerically from $\xi = 0$ to $\xi = Pl/pR^3$. The boundary condition at the root, $x = l$, ($\xi = Pl/pR^3$), was taken as $\zeta = 0$. Curve C in Fig. 2 gives the dimensionless tip deflection due to shear as $(tEd_s/pR^2) = \zeta_0$, where ζ_0 is the value of ζ when $\xi = 0$. The total tip deflection is the sum of that due to bending, curve A, and that due to shear, curve C.

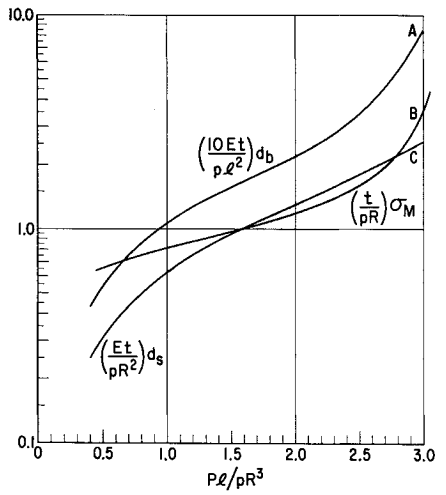

Fig. 2 Cantilever beam with a tip load

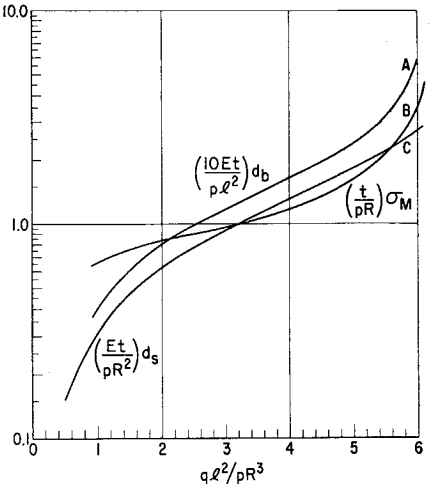

Fig. 3 Cantilever beam with a uniform load

B. *Beam with a uniform load*

The analysis and numerical integration for a uniformly loaded beam was similar to that for a tip-loaded beam. The results obtained are shown in Fig. 3.

III. Examples

1) Consider an inflated circular-cylindrical cantilever beam with wall thickness $t = 0.001$ in., length $l = 132$ in., radius $R = 12$ in., modulus $E = 550{,}000$ lb/in.^{2}, internal pressure $p = 0.325$ lb/in.^{2}, and lateral tip load $P = 12$ lb. The dimensionless load $Pl/pR^3 = 2.82$ is computed. From Fig. 2, curve A, $(Et/pl^2)d_b = 0.553$, giving $d_b = 5.69$ in. From Fig. 2, curve C, $(Et/pR^2)d_s = 2.3$, giving $d_s = 0.20$ in. The total deflection is therefore $d_b + d_s = 5.89$ in. From Fig. 2, curve B, $(t/pR)\sigma_M = 2.26$, giving a maximum stress $\sigma_M = 8800$ lb/in^2.

2) Consider the cylinder of example 1 with $P = 15$ lb and $p = 0.542$ lb/in^2. The dimensionless load $Pl/pR^3 = 2.11$. From Fig. 2, curve A, $(Et/pl^2)d_b = 0.227$, giving $d_b = 3.88$ in. From Fig. 2, curve C, $(Et/pR^2)\ d_s = 1.40$, giving $d_s = 0.20$ in. The total deflection is therefore $d_b + d_s = 4.08$ in. From Fig. 2, curve B, $(t/pR)\sigma_M = 1.27$, giving a maximum stress $\sigma_M = 8300$ lb/in^2.

3) Consider the cylinder of example 1 with a uniformly distributed lateral load of $ql = 24$ lb. The dimensionless load $ql^2/pR^3 = 5.64$ is computed. From Fig. 3, curve A, $(Et/pl^2)\ d_b = 0.371$, giving $d_b = 3.82$ in. From Fig. 3, curve C, $(Et/pR^2)\ d_s = 1.37$, giving $d_s = 0.12$ in. The total deflection is therefore $d_b + d_s = 3.94$ in. From Fig. 3, curve B, $(t/pR)\ \sigma_M = 2.26$, giving a maximum stress $\sigma_M = 8800$ lb/in^2.

IV. Conclusions

An analysis has been presented for the deflection of inflated cylindrical cantilever beams. The results are given in chart form for the tip deflection and maximum stress. The results are in agreement with earlier results for the load at which incipient bulking is initiated and for the collapse load.

References

[1] Leonard, R. W., Brooks, G. W., and McComb, H. G., Jr., "Structural considerations of inflatable re-entry vehicles," NASA TN D-457 (September 1960).

[2] Stein, M. and Hedgepeth, J. M., "Analysis of partly wrinkled membranes," NASA TN D-813 (July 1961).

[3] Topping, A. D., "A preliminary study of methods of analysis

of airwall structures," Goodyear Aircraft Corp., GER5850 (February 19, 1954).

[4] Harris, J. T. and Stimler, F. J., "Expandable structures for space," Astronautics 6, 30 (April 1961).

[5] Darevskii, V. M., "Stability of a console cylindrical shell under bending by a transverse force with twisting and internal pressure," ARS J. 31, 125–133 (1961).

[6] Hopkins, H. G. and Brown, E. H., "The effect of internal pressure on the initial buckling of thin-walled circular cylinders under torsion," Ames Research Center, Rept. and Memo. 2423 (1951).

[7] Peterson, J. P., "Correlation of the buckling strength of pressurized cylinders in compression or bending with structural parameters," NASA TN D-526 (October 1960).

[8] Harris, L. A., Suer, S. H., Skene, W. T., and Benjamin, R. J., "The stability of thin-walled unstiffened circular cylinders under axial compression including the effects of internal pressure," J. Aeronaut. Sci. 24, 587–596 (1957).

[9] Lo, H., Crate, H., and Schwartz, E. B., "Buckling of thin-walled cylinder under axial compression and internal pressure," NACA TN 1027 (1951).

[10] Fung, V. C. and Sechler, E. E., "Buckling of thin-walled circular cylinders under axial compression and internal pressure," J. Aeronaut. Sci. 24, 351–356 (1957).

Minimum Altitude Variation Orbits about an Oblate Planet

FORD KALIL*
The Martin Company, Baltimore, Md.

Introduction

THE general problem of satellite motion over an oblate earth has been studied at length, and the literature is too extensive to list here. The study used in this work is that of Struble.[1] In addition, Rider[2] has studied a "Class of Minimum Altitude Variation Orbits About an Oblate Earth," in which case the resulting orbits were essentially of zero eccentricity. Rider uses the results obtained by Fosdick[3] for the motion of a near-earth satellite. However, the problem of maintaining a minimum satellite altitude variation during certain phases of satellite motion and for a short orbital life has not been reported in the literature.

A satellite orbit that closely follows the contour of the oblate earth during one-quarter of a revolution could be useful, first, in studying the flattening of the atmosphere, which is usually assumed to have the same flattening as the earth because density variations can be measured more accurately than the absolute value. Hence, a null method of measurement for verifying this assumption probably could be used to advantage. Secondly, such an orbit could be useful in photographic missions because the camera's resolution is best at the altitude for which the optical system is preset, and thus the degradation of the resolution is minimized when the altitude variations are minimized.

The purpose of this study is to derive a method and corresponding analytical expressions for determining the orbital parameters for an orbit that closely follows the contour of the earth during one-quarter of each revolution with a minimum altitude variation throughout an operational time of several days. In this work, the first-order theory of Struble was used. A cursory study indicates that such a class of orbits is quite feasible.

The effects of atmospheric drag decay by an oblate, rotating atmosphere on orbits whose $0 \leq e \leq 0.01$ have been studied.[4–10] For an $\bar{h} \simeq 100$ naut miles, $e \simeq 0.0022$ (the e for minimum altitude variation over one-quarter of each orbit revolution), and $B = (C_D A/2m) = 1$, one has $\Delta a/\text{rev} \cong 0.6$ naut mile per revolution, and $\Delta e/\text{rev} \cong 3 \times 10^{-7}$. Since the actual ballistic coefficient B is generally significantly less than 1, it safely can be said that, for short-term missions, the effect of drag is negligible for all practical purposes.

Theory

The earth's local radius R is given to within about 92 ft by

$$R = R_e(1 - f \sin^2\theta) \tag{1}$$

where

$$\sin^2\theta = \sin^2 i_0 \sin^2\beta \tag{2}$$

and θ = geocentric latitude, $f = 1/298.25$ = earth's flattening, and R_e = earth's equatorial radius.

The local satellite altitude h_β above the earth's surface is given by

$$h_\beta = r - R \tag{3}$$

where r is the local satellite orbital radius, measured from the earth's center. For a Keplerian orbit, r is given by

$$r = \frac{a(1 - e^2)}{1 + e\cos(\beta - \omega)} \tag{4}$$

where a is the semimajor axis an l e is the eccentricity.

Since there was no a priori knowledge of the magnitude of e, the Keplerian orbit was examined first. It was found that $e = 0(J)$ for orbits in which the satellite is to follow the contour of the earth during one-quarter of a revolution, making it permissible to drop terms involving e^2 or Je in the first-order theory.

Using Struble's results, the satellite radial position from the earth's center is given by

$$1/r = (1/\bar{r}_0)[1 + e\cos(\beta - \omega) - Jv] \tag{5}$$

where $\bar{r}_0$ and e are arbitrary constants, and

$$v = \frac{1}{12}\left(\frac{R_e}{\bar{r}_0}\right)^2 \sin^2 i_0 \left[\left(2 + \frac{e^2}{3}\right)\cos 2\beta + e\cos(3\beta - \omega) + \frac{e^2}{6}\cos(4\beta - 2\omega) + \frac{3e^2}{2}\cos 2\omega\right] + \frac{1}{12}\left(\frac{R_e}{\bar{r}_0}\right)^2 e^2(2 - 3\sin^2 i_0)\cos(2\beta - 2\omega) \tag{6}$$

$$d\omega/d\beta = (J/2)(R_e/\bar{r}_0)^2(5\cos^2 i_0 - 1) \tag{7}$$

The instantaneous line of nodes regresses at a variable rate, and to first order is given by

$$\Omega = J(R_e/\bar{r}_0)^2 \cos i_0[\beta - \tfrac{1}{2}\sin 2\beta + e\sin(\beta - \omega) - \tfrac{1}{6}e\sin(3\beta - \omega) - \tfrac{1}{2}e\sin(\beta + \omega)] \tag{8}$$

From Eqs. (7) and (8), the secular variations in ω and Ω, respectively, are given by

$$\dot{\omega}\frac{\text{deg}}{\text{rev}} = 360\left(\frac{J}{2}\right)\left(\frac{R_e}{\bar{r}_0}\right)^2(5\cos i_0 - 1) \tag{9}$$

$$\dot{\Omega}\frac{\text{deg}}{\text{rev}} = -360J\left(\frac{R_e}{\bar{r}_0}\right)^2 \cos i_0 \tag{10}$$

where a satellite revolution is defined as extending from one ascending node to the next.

In these expressions, ω is the argument of perigee, β is the central angle in the orbital plane measured from the mean line of nodes, i_0 is the mean angle of incidence of the orbital plane, and $J = 1.6235 \times 10^{-3}$ is the coupling coefficient of the second harmonic in the earth's gravitational potential.

Since J is of the order of 10^{-3}, then for small e (i.e., e of the

Received by ARS October 2, 1962; revision received March 29, 1963.

* Design Engineer, Space Systems Division.